Properties of quark matter and hybrid stars from a quasiparticle model

He Liu,* Yong-Hang Yang, Yue Han, and Peng-Cheng Chu†

Science School, Qingdao University of Technology, Qingdao 266000, China
and The Research Center of Theoretical Physics, Qingdao University of Technology, Qingdao 266033, China

(Received 24 February 2023; accepted 11 July 2023; published 3 August 2023)

We investigate the global properties of hybrid stars and quark-matter cores by using a quasiparticle model that rules out the possibility of the existence of absolutely stable strange quark matter within the hybrid stars. Results from our study indicate that the coupling constant g can stiffen the equation of state of hybrid star matter and thus increase the hybrid star maximum mass and its tidal deformability, whereas it also decreases the mass and radius of the pure quark. By breaking the absolutely stable condition, we provide the maximum mass, minimum radius $R_{1.4}$, and minimum tidal deformation $\Lambda_{1.4}$ of the hybrid stars as well as the maximum mass and radius of the quark-matter core with different g values within the allowable regions (the energy per nucleon of both u-d quark matter and strange quark matter must exceed 930 MeV) on the g-$B^{1/4}$ plane. In addition, we find that a step change of the sound velocity occurs in the hadron-quark mixed phase, and the approximate rule that the polytropic index $\gamma \leq 1.75$ can also be used as a criterion for separating hadronic from quark matter in our work. Our results also confirm that the sizable quark-matter cores ($R_{QC} > 6.5$ km) containing the mixed phase can appear in $2M_\odot$ massive stars.

DOI: 10.1103/PhysRevD.108.034004

I. INTRODUCTION

Understanding the nature of the strongly interacting matter, especially the possible existence of phase transition, is a major thrust of current research in both nuclear physics and astrophysics. It is generally believed that a first-order phase transition from the hadronic to quark matter at high baryon densities may occur in the interior of massive neutron stars [1–3]. Some recent studies, for instance, have also shown that quark-matter cores can appear in massive neutron stars [4], and the presence of a first-order phase transition from hadronic to quark matter can imprint signatures in binary merger observations [5,6], as well as that the sudden decrease in the gravitational-wave frequency in the binary-neutron-star merger simulations is closely related to the hadron-quark phase transition [7]. The appearance of quark matter in massive stars is considered a hot topic in compact object studies, and the neutron stars with a hadron mantle and a quark core are usually referred to as hybrid stars. Hence, observations of massive neutron stars can provide us with a valuable window into an otherwise inaccessible realm of quark matter.

Some inspiring progress over the last several years has been made in neutron star observations, and thus in our understanding of the equation of state (EOS) of neutron star matter. The measurements of PSR J1614-2230 and PSR J0348 + 0432 have led to a precise determination of $1.908 \pm 0.016 M_\odot$ [8–10] and $2.01 \pm 0.04 M_\odot$ [11] for their respective masses. More recently, the first simultaneous measurements of the mass and radius of a neutron star using the Neutron Star Interior Composition Explorer (NICER) data were those of the millisecond pulsar PSR J0030 + 0451. The two independent analyses predict (68% credible interval) $M = 1.34^{+0.15}_{-0.16} M_\odot$, $R = 12.71^{+1.14}_{-1.19}$ km [12] and $M = 1.44^{+0.15}_{-0.14} M_\odot$, $R = 13.02^{+1.24}_{-1.06}$ km [13]. PSR J0740 + 6620 has a gravitational mass of $2.08 \pm 0.07 M_\odot$, which is considered the highest reliably determined neutron star mass [14–16]. Its radius was determined using the NICER and xray multimirror data with the results for the radius $12.39^{+1.30}_{-0.98}$ [15] and $13.71^{+2.61}_{-1.50}$ km [16] (68% credible interval). And the radius range that spans the $\pm 1\sigma$ credible intervals of all the radius estimates in the different frameworks is 12.45 ± 0.65 km for a canonical mass $M = 1.4 M_\odot$ neutron star [16]. The gravitational-wave events GW170817 [17] and GW190814 [18] have provided more additional constraints on the EOS of neutron star matter. In Ref. [17], the LIGO-Virgo Collaboration investigated the properties of the tidal deformability of compact stars and set an upper limit of $\Lambda_{1.4} < 800$ for the low-spin priors of 1.4 solar mass pulsars. The improved analysis of GW170817 by the LIGO-Virgo Collaboration has found with a 90% confidence the tidal deformability of the merging neutron stars constrained to be the range $70 < \Lambda_{1.4} < 580$ [19]. Additionally, the newly discovered neutron binary merger GW190814 which has a secondary component of mass

*liuhe@qut.edu.cn
†kyois@126.com

$(2.50 \sim 2.67)M_\odot$ at a 90% credible level has also aroused lots of debates on whether the candidate for the secondary component is a neutron star or a light black hole [18]. These observation events/objects comprise the multimessenger dataset for our following analyses on the properties of neutron star matter.

The existence of such high-mass neutron stars indicates that the EOS of neutron star matter is relatively stiff, whereas the tidal deformation in gravitational-wave observations of GW170817 implies a soft EOS at the intermediate density range [16]. The radius of a $1.4M_\odot$ star is known to be most sensitive to the variation of pressure around $1 \sim 2\rho_0$ [20,21]. Recent measurements of the massive compact stars PSR J0030 + 0451 and PSR J0740 + 6620 have significantly tightened the EOS at densities between $1.5\rho_0$ and $5.0\rho_0$ [13,16]. In addition, the EOS of strongly interacting matter at densities $2\rho_0 < \rho < 5\rho_0$ has also been constrained by the measurements of collective flows [22] and subthreshold kaon production [23] in relativistic heavy-ion collisions. When taken together, these observations and the experimental information have already narrowed significantly the EOS range of allowed theoretical models. Recent work on the EOS by effective models has generally concluded that the EOS of neutron star matter must be moderately soft at intermediate densities and stiff enough at high densities, which is highly relevant to a possible phase transition to quark matter [24–29].

In the present study, the neutron stars could be converted to hybrid stars with the hadron-quark phase transition. We describe strange quark matter (SQM) in hybrid stars based on the quark quasiparticle model, and nuclear matter using an improved isospin- and momentum-dependent interaction (ImMDI) model. The ImMDI model is constructed from fitting cold nuclear matter properties at saturation density and the empirical nucleon optical potential [30,31], and it has been extensively used in intermediate energy heavy-ion reactions to study the properties of nuclear matter. The Gibbs construction [32] is adopted for the description of hadron-quark mixed phase, where the coexisting hadronic and quark phases need to satisfy the β-equilibrium and charge-neutral conditions. On the other hand, the Witten hypothesis suggests that the absolutely stable SQM is the true ground state of nuclear matter, which implies that a hybrid star containing a sufficient amount of SQM in its core will rapidly convert into a strange quark star [33–35]. Some previous studies on the EOS of hybrid star matter using various models with the Gibbs construction and modified bag constants [36–38] simply do not consider the absolute stability condition as a prerequisite for quark matter in hybrid stars, rather than ruling out the possibility of the existence of absolutely stable SQM. In this work, we will examine the global properties of hybrid stars and quark-matter cores by excluding absolutely stable SQM inside hybrid stars.

This paper is organized as follows. In Sec. II, we describe the quasiparticle model with different parameter sets for the quark matter at zero temperature. We present in Sec. III the global properties of hybrid stars and quark-matter cores by excluding absolutely stable SQM, such as the EOS, the sound velocity c_s^2, and the polytropic index γ; the mass-radius relation and the dimensionless tidal deformability of hybrid stars, as well as the mass-radius relation of quark-matter cores. Our conclusions are given in Sec. IV.

II. THE THEORETICAL MODEL

The hybrid EOS consists of a hadronic phase connected to a quark phase through a hadron-quark mixed phase. The possible appearance of hyperons is neglected, which is due to the fact that there are still large uncertainties on the hyperon-nucleon (YN) and hyperon-hyperon (YY) interactions in the nuclear medium [39,40]. Besides, following the results from Ref. [37], the fraction of hyperons disappears quickly in hadron-quark mixed phase, which means that the effect of hyperons at high densities, especially in the hadron-quark mixed phase, is expected to be small. Thus, we mainly focus on the properties of hybrid star matter without hyperons in this work.

Here we want to apply an ideal gas of quasiparticles with effective masses to the case of strange quark matter. The effective quark masses are derived from the zero momentum limit of the dispersion relations following from an effective quark propagator obtained from resumming one-loop self energy diagrams in the hard dense loop approximation at finite chemical potential [41]. And the effective quark mass for each flavor of quarks in quasiparticle model at zero temperature can be expressed as [42–44]

$$m_q = \frac{m_{q0}}{2} + \sqrt{\frac{m_{q0}^2}{4} + \frac{g^2\mu_q^2}{6\pi^2}}, \tag{1}$$

where m_{q0} is the current mass for three flavor quarks, which is set as $m_{u0} = 5.5$ MeV, $m_{d0} = 5.5$ MeV, and $m_{s0} = 95$ MeV respectively in this work [44,45]. μ_q means the chemical potential for the different flavor of quarks, and g represents the coupling constant of the strong interaction. In principle the value of g should be determined as a μ-dependent running coupling constant from the renormalization group equation at finite density. However, so far there are no clear results at finite temperature or density [46], and thus g is taken as a free parameter ranging from 1 to 5.

The quasiparticle contribution to the thermodynamic potential density for SQM can be written as

$$\Omega = \sum_{q=u,d,s} [\Omega_q + B_q(\mu_q)] + B, \tag{2}$$

where Ω_q in the sum shows the contribution to the thermodynamic potential density for all flavors of quarks

(u, d, and s), $B_q(\mu_q)$ is the additional terms for quarks, which is defined as a necessary energy counterterm in order to maintain thermodynamic self-consistency [47], and B denotes the phenomenological bag constant which corresponds to the negative vacuum pressure term for nonperturbative confinement [48]. The expression of Ω_q at temperature $T = 0$ and chemical potential μ_q for the quasiparticle of mass m_q can be written as

$$\Omega_q = -\frac{d_q}{24\pi^2}\left[\mu_q k_{Fq}\left(\mu_q^2 - \frac{5}{2}m_q^2\right) + \frac{3}{2}m_q^4 \ln\left(\frac{k_{Fq}+\mu_q}{m_q}\right)\right], \tag{3}$$

where d_q denotes the degree of degeneracy (e.g., $d_q = 6$ for quarks), and the Fermi momentum is $k_{Fq} = (\mu_q^2 - m_q^2)^{1/2}$. The term $B_q(\mu_q)$ is determined as

$$B_q(\mu_q) = -\int \frac{\partial\Omega_q}{\partial m_q}\frac{\partial m_q}{\partial \mu_q}d\mu_q. \tag{4}$$

The pressure P_Q and energy density ε_Q of SQM are, respectively, given by

$$P_Q = -\sum_{q=u,d,s}[\Omega_q + B_q(\mu_q)] - B, \tag{5}$$

$$\varepsilon_Q = \sum_{q=u,d,s}\mu_q\rho_q - P_Q, \tag{6}$$

where ρ_q stands for the net quark number density. In the quark phase, the system is composed of a mixture of quarks (u, d, and s) and leptons (e and μ) under the charge neutrality condition

$$\frac{2}{3}\rho_u - \frac{1}{3}(\rho_d + \rho_s) - \rho_e - \rho_\mu = 0, \tag{7}$$

and the β-equilibrium condition

$$\mu_s = \mu_d = \mu_u + \mu_e, \tag{8}$$

$$\mu_\mu = \mu_e. \tag{9}$$

In terms of the electron mass $m_e = 0.511$ MeV and the muon mass $m_\mu = 106$ MeV, the lepton contributions to the energy density and the pressure are

$$\varepsilon_L = \sum_{i=e,\mu}\frac{1}{\pi^2}\int_0^{k_{Fi}}\sqrt{p^2+m_i^2}\,p^2dp, \tag{10}$$

$$P_L = \sum_{i=e,\mu}\mu_i\rho_i - \varepsilon_L, \tag{11}$$

where $k_{Fi} = (3\pi^2\rho_i)^{\frac{1}{3}}$ is the lepton Fermi momentum. The total energy density and pressure including the contributions from both quarks and leptons in quark phase are given by

$$\varepsilon^Q = \varepsilon_Q + \varepsilon_L, \tag{12}$$

$$P^Q = P_Q + P_L. \tag{13}$$

In the hadronic phase, an ImMDI model is used to describe the β-equilibrium and charge-neutral nuclear matter. In our previous study [29], the ImMDI model is fitted to the properties of cold symmetric nuclear matter (SNM), which is approximately reproduced by the self-consistent Greens function approach [49,50] or chiral effective many-body pertubation theory [51,52]. The potential energy density from the ImMDI model is then given by [29,30]

$$\begin{aligned} V_{\mathrm{ImMDI}} = {} & \frac{A_u\rho_n\rho_p}{\rho_0} + \frac{A_l}{2\rho_0}(\rho_n^2+\rho_p^2) \\ & + \frac{B}{\sigma+1}\frac{\rho^{\sigma+1}}{\rho_0^\sigma}\times(1-x\delta^2) + \frac{1}{\rho_0}\sum_{\tau,\tau'}C_{\tau,\tau'} \\ & \times\iint d^3\vec{p}\,d^3\vec{p}\,'\frac{f_\tau(\vec{r},\vec{p})f_{\tau'}(\vec{r}',\vec{p}')}{1+(\vec{p}-\vec{p}')^2/\Lambda^2}, \end{aligned} \tag{14}$$

where ρ_n and ρ_p are the neutron and proton number densities, respectively; $\rho_0 = 0.16$ fm^{-3} is the saturation density of nuclear matter; $\delta = (\rho_n - \rho_p)/\rho$ is the isospin asymmetry of nuclear matter with $\rho = \rho_n + \rho_p$; and $f_\tau(\vec{r},\vec{p})$ is the nucleon phase-space distribution function from the Wigner transformation of its density matrix with $\tau = 1(-1)$ for neutrons (protons) being the isospin index. The parameter set (A_l, A_u, B, $C_l = C_{\tau,\tau}$, $C_u = C_{\tau,-\tau}$, Λ, σ) can be fitted by seven empirical constraints, i.e., five isoscalar constraints of the saturation density ρ_0, the binding energy E_0, the incompressibility K_0, the isoscalar effective mass $m_s^\star$, and the single-particle potential $U_{0,\infty}$ at infinitely large nucleon momentum in symmetric nuclear matter, as well as two isovector constraints of the symmetry energy $E_{\mathrm{sym}}(\rho_0)$ and the symmetry potential $U_{\mathrm{sym},\infty}$ at infinitely large nucleon momentum. In Refs. [29,30], an optimized parameter set (A_0, B, C_{l0}, C_{u0}, Λ, σ, x, y, z) was introduced by using the following relations:

$$\begin{aligned} A_l(x,y) &= A_0 + y + x\frac{2B}{\sigma+1}, \\ A_u(x,y) &= A_0 - y - x\frac{2B}{\sigma+1}, \\ C_{\tau,\tau}(y) &= C_{l0} - 2(y-2z)\frac{p_{f0}^2}{\Lambda^2\ln[(4p_{f0}^2+\Lambda^2)/\Lambda^2]}, \\ C_{\tau,-\tau}(y) &= C_{u0} + 2(y-2z)\frac{p_{f0}^2}{\Lambda^2\ln[(4p_{f0}^2+\Lambda^2)/\Lambda^2]}, \end{aligned} \tag{15}$$

where p_{f0} is the nucleon Fermi momentum in SNM at saturation density. In the above relations, the parameters x, y, and z are introduced to adjust the slope $L(\rho)$ of symmetry energy, the momentum dependence of the symmetry potential, and the symmetry energy $E_{\rm sym}(\rho_0)$ at saturation density, respectively.

Recently, the discovery of GW170817 has triggered many analyses of neutron star observables to constrain nuclear symmetry energy. The average value of the slope parameter of the symmetry energy L from the 24 new analyses of neutron star observables since GW170817 was about $L = 57.7 \pm 19$ MeV at a 68% confidence level [53], which is consistent with the latest report of the slope parameter L between 42 and 117 MeV from studying the pion spectrum ratio in heavy-ion collision in an experiment performed at RIKEN [54]. However, the lead radius experiment (PREX-II) reported very recently new constraints on the neutron radius of ^{208}Pb, which implies a neutron skin thickness of $R_{\rm skin}^{^{208}{\rm Pb}} = 0.283 \pm 0.071$ fm [55] and constrains the slope parameter to $L = 106 \pm 37$ MeV [56], which is much larger than many previous constraints from microscopic calculations or experimental measurements [53,57,58]. In order to better focus on the properties of quark matter, we thus choose for the hadronic phase a fixed parameter set, $x = -0.3$, $y = 32$ MeV, and $z = 0$, that would allow $2.08M_\odot$ neutron stars and still satisfy well nuclear matter constraints at saturation density, i.e., the binding energy $E_0(\rho_0) = -15.9$ MeV, the incompressibility $K_0 = 240$ MeV, the symmetry energy $E_{\rm sym}(\rho_0) = 32.5$ MeV, the slope parameter $L = 106$ MeV, the isoscalar effective mass $m_s^\star = 0.7m$, and the single-particle potential $U_{0,\infty} = 75$ MeV at infinitely large nucleon momentum.

In the mean-field approximation, Eq. (14) leads to the following single-particle potential [29,30]:

$$\begin{aligned} U_\tau(\rho,\delta,\vec{p}) = {} & A_u\frac{\rho_{-\tau}}{\rho_0} + A_l\frac{\rho_\tau}{\rho_0} \\ & + B\frac{\rho^\sigma}{\rho_0}(1-x\delta^2) - 4x\tau\frac{B}{\sigma+1}\frac{\rho^{\sigma-1}}{\rho_0^\sigma}\delta\rho_{-\tau} \\ & + \frac{2C_l}{\rho_0}\int d^3\vec{p}\,'\frac{f_\tau(\vec{r},\vec{p})}{1+(\vec{p}-\vec{p}\,')^2/\Lambda^2} \\ & + \frac{2C_u}{\rho_0}\int d^3\vec{p}\,'\frac{f_{-\tau}(\vec{r},\vec{p})}{1+(\vec{p}-\vec{p}\,')^2/\Lambda^2}. \end{aligned} \tag{16}$$

The chemical potential of neutrons and protons can be calculated from

$$\mu_\tau = \sqrt{m^2 + p_f^{\tau 2}} + U_\tau(p_f^\tau), \tag{17}$$

with the nucleon mass m and the Fermi momentum $p_f^\tau = (3\pi^2\rho_\tau)^{1/3}$. The total energy density and pressure of the hadron phase can be written as

$$\varepsilon^H = \varepsilon_H + \varepsilon_L, \tag{18}$$

$$P^H = P_H + P_L, \tag{19}$$

where ε_H and P_H, respectively, are the energy density and pressure of baryons. The detailed form can be written as

$$\begin{aligned} \varepsilon_H &= V_{HP} + V_{HK} + V_{HM}, \\ P_H &= \sum_\tau \mu_\tau\rho_\tau - \varepsilon_H, \end{aligned} \tag{20}$$

where V_{HP} is the potential energy density of baryons calculated from $V_{\rm ImMDI}$, and V_{HK} and V_{HM} are, respectively, the kinetic energy and mass contributions given by

$$\begin{aligned} V_{HK} &= \sum_\tau \frac{p_f^{\tau 5}}{10\pi^2 m_\tau}, \\ V_{HM} &= \sum_\tau \rho_\tau m_\tau. \end{aligned} \tag{21}$$

The hadron-quark mixed phase is predicted to exist in the region between hadronic matter and quark matter based on various theoretical approaches. In the Maxwell construction, the coexisting hadronic and quark phases have equal pressure and baryon chemical potential but different electron chemical potential. The Gibbs construction is more generally adopted for the description of the hadron-quark mixed phase, where the coexisting hadronic and quark phases are allowed to be charged separately. Besides, the mixed phase in the Gibbs construction persists within a limited pressure range, so it is convenient to form a massive neutron star containing the mixed phase. Both of the Maxwell and Gibbs constructions involve only bulk contributions, but the finite-size effects like surface and Coulomb contributions are neglected. The possible geometrical structure of the mixed phase has been extensively discussed in Refs. [59–63]. However, the large uncertainties in the structure and density range of the mixed phase are still present. In the present work, the hadron-quark mixed phase is described by imposing the Gibbs construction [1,32]: $T^H = T^Q$, $P^H = P^Q$, $\mu_B^H = \mu_B^Q$, and $\mu_c^H = \mu_c^Q$, where μ_B and μ_c are the baryon and charge chemical potential, as well as the labels H and Q representing the hadronic and quark phases, respectively. Adding baryon number conservation and charge neutrality conditions, the dense matter enters the mixed phase, in which the hadronic and quark matter need to satisfy following equilibrium conditions:

$$\begin{aligned} &\mu_i = \mu_B b_i - \mu_c q_i, \qquad P^H = P^Q, \\ &\rho_B = (1-Y)(\rho_n+\rho_p) + \frac{Y}{3}(\rho_u+\rho_d+\rho_s), \\ &0 = (1-Y)\rho_p + \frac{Y}{3}(2\rho_u - \rho_d - \rho_s) - \rho_e - \rho_\mu, \end{aligned} \tag{22}$$

where Y is the baryon number fraction of the quark phase. The crust of hybrid stars, in our calculations, is considered to be divided into two parts: the inner and the outer crust as in the previous treatment [64,65]. The polytropic form $P = a + b\varepsilon^{4/3}$ has been found to be a good approximation to the inner crust EOS [66], and the outer crust usually consists of heavy nuclei and electron gas, where we use the EOS in Ref. [67].

Using the whole EOS from hadronic to quark phase, the mass-radius relation of hybrid stars can be obtained by solving the Tolman-Oppenheimer-Volkoff (TOV) equation, which can be written as

$$\frac{dP(r)}{dr} = -\frac{M(r)[\varepsilon(r)+P(r)]}{r^2}\left[1+\frac{4\pi P(r)r^3}{M(r)}\right] \times \left[1-\frac{2M(r)}{r}\right]^{-1}, \tag{23}$$

where $\varepsilon(r)$ is the energy density and $P(r)$ is the pressure obtained from the equation of state. $M(r)$ is the gravitational mass inside the radius r of the hybrid star given by

$$\frac{dM(r)}{dr} = 4\pi r^2 \varepsilon(r). \tag{24}$$

The gravitational waves emitted from the merger of two neutron stars are considered as another probe to the EOS of dense matter [68,69]. The tidal deformability Λ of neutron stars during their merger is related to the Love number k_2 through the relation $k_2 = 3/2\Lambda\beta^5$ [68,70], which can be given by

$$\begin{aligned} k_2 =& \frac{8}{5}\beta^5(1-2\beta)^2[2-y_R+2\beta(y_R-1)] \\ &\times\{2\beta[6-3y_R+3\beta(5y_R-8)] \\ &+4\beta^2[13-11y_R+\beta(3y_R-2)+2\beta^2(1+y_R)] \\ &+3(1-2\beta)^2[2-y_R+2\beta(y_R-1)]\ln(1-2\beta)\}^{-1}, \end{aligned} \tag{25}$$

where $\beta \equiv M/R$ is the compactness of the star, and $y_R \equiv y(R)$ is the solution at the neutron star surface to the first-order differential equation

$$r\frac{dy(r)}{dr} + y(r)^2 + y(r)F(r) + r^2Q(r) = 0, \tag{26}$$

with

$$\begin{aligned} F(r) &= \frac{r-4\pi r^3[\varepsilon(r)-P(r)]}{r-2M(r)}, \\ Q(r) &= \frac{4\pi r\left[5\varepsilon(r)+9P(r)+\frac{\varepsilon(r)+P(r)}{\partial P(r)/\partial\varepsilon(r)}-\frac{6}{4\pi r^2}\right]}{r-2M(r)} \\ &\quad -4\left[\frac{M(r)+4\pi r^3P(r)}{r^2(1-2M(r)/r)}\right]^2. \end{aligned} \tag{27}$$

For a given central density ρ_c and using the boundary conditions in terms of $y(0) = 2$, $P(0) = P_c$, $M(0) = 0$, and $\varepsilon(0) = 0$, the mass M, radius R, and the tidal deformability Λ can be obtained once an EOS is supplied.

III. RESULTS AND DISCUSSIONS

The absolutely stable condition of SQM has been proposed in Ref. [71], which can put very strict constraints on the parameter space for most of the phenomenological quark-matter models. The ordinary nuclei are made of nucleons and not of a two-flavor quark phase, the energy per nucleon (E/A) of $u-d$ quark matter (udQM) therefore must exceed the lowest energy per nucleon found in nuclei, which is about 930 MeV for iron ($M(^{56}\mathrm{Fe}/56)$). For the strange quark matter, Ref. [71] points out SQM in aggregates large enough that surface effects can be ignored and that electrons (or positrons) bound to it by Coulomb forces are inside the chunk and numerous enough to be treated as a degenerate Fermi gas. This requires E/A of SQM to be less than that of the nucleon ($M_N = 939$ MeV). Actually for E/A between 930 and 939 MeV SQM could decay by emission of nuclei accompanied by weak interactions to maintain flavor equilibrium, which means that the minimum value of E/A of the absolutely stable SQM at zero temperature should be less than 930 MeV. However, the hypothesis of absolutely stable SQM (or "Witten hypothesis") suggests that the energy required to create a single strange quark could be offset by the energy released when two up or down quarks combine with a strange quark to form a lower-energy state, which would imply that the absolutely stable SQM is the ground state of matter, and that all forms of matter would eventually decay into SQM [33–35]. In this case, a hybrid star containing a sufficient amount of SQM in its core will rapidly convert into a strange quark star. Thus, the SQM in hybrid stars should break the absolutely stable condition, and the energy per nucleon (E/A) of both udQM and SQM must exceed the lowest energy per nucleon 930 MeV.

We first present in Fig. 1 the energy per nucleon and corresponding pressure of SQM and udQM as functions of baryon number density in the quasiparticle model with five different parameter sets: $g = 1, B^{1/4} = 157.0$ MeV; $g = 2$, $B^{1/4} = 153.0$ MeV; $g = 3$, $B^{1/4} = 146.0$ MeV; $g = 4$, $B^{1/4} = 135.5$ MeV; and $g = 5$, $B^{1/4} = 120.0$ MeV. These parameter sets include various values for the coupling constant g and bag constant $B^{1/4}$. However, it should be noted that all the minimum values of energy per nucleon of SQM and udQM are larger than 930 MeV in all of the five parameter settings, which is due to the break in absolute stability for quark matter. We have ensured that the minimum value of energy per nucleon of SQM is only slightly larger than 930 MeV in our parameter settings, but the minimum value of energy per nucleon actually increases with increasing bag constant B while fixing the

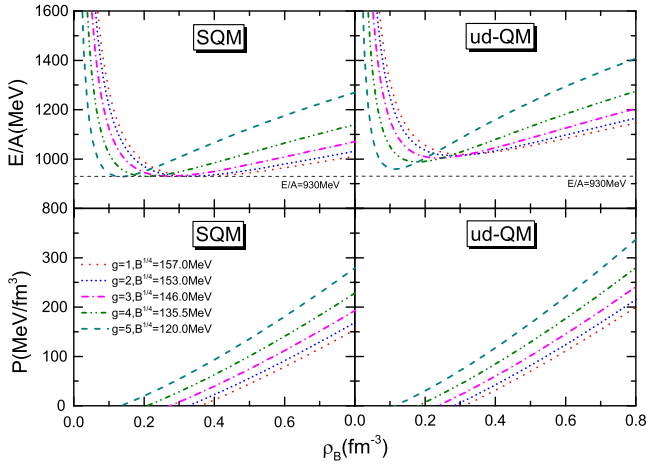

FIG. 1. The energy per nucleon (E/A) and the corresponding pressure as functions of the baryon density for SQM (left panels) and udQM (right panels) at zero temperature from the quasiparticle model with different parameter sets. The horizontal dashed line $E/A = 930$ MeV is also shown for comparison.

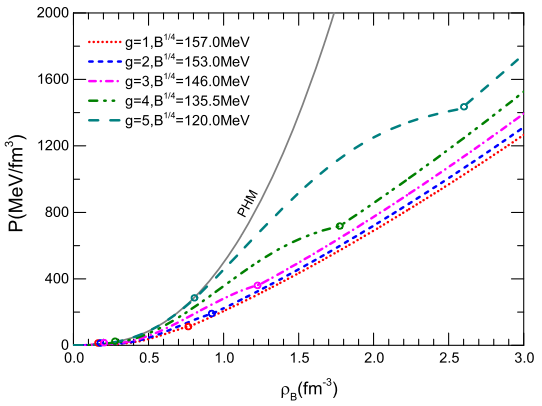

FIG. 2. EOS, pressure as a function of the baryon density, of hybrid star matter based on the ImMDI interaction for nuclear matter with a fixed parameter set ($x = -0.3$, $y = 32$ MeV, and $z = 0$) and the quasiparticle model for SQM with different parameter sets. The two cycles with same color represent the range of the hadron-quark mixed phase, and the result from pure hadronic matter (PHM) is also shown for comparison.

coupling constant g. Therefore, the value of B in our present parameter sets is the minimum value. It is important to consider that the ranges of B and g can significantly impact the properties of SQM and hybrid stars, which will be further discussed later in this work. Furthermore, it can be seen from Fig. 1 that the baryon density of the minimum energy per nucleon for SQM and udQM in all cases corresponds exactly to the zero pressure points, satisfying the thermodynamic self-consistency of quark matter. Although the baryon density of the zero pressure point decreases with the coupling constant g, the equation of state containing SQM/udQM becomes stiffer, which can support more massive hybrid stars.

We show in Fig. 2 the EOS of hybrid star matter with the hadron-quark phase transition in different parameter sets. The ImMDI interaction with a fixed parameter set, $x = -0.3$, $y = 32$ MeV, and $z = 0$, is used for nuclear matter, and the two cycles with the same color in Fig. 2 represent the range of the hadron-quark mixed phase. It can be seen that the phase transition leads to a softening of EOS of hybrid star matter, compared with their purely hadronic counterpart. Moreover, the EOS of hybrid star matter is sensitive to the strength of the coupling constant g. With increasing the coupling constant g for SQM the EOS of hybrid star matter becomes stiffer, which is consistent with the results of strange quark star matter in Ref. [45], and the onset of the phase transition is moving to higher densities since the transition pressure is also increasing under the Gibbs construction. It should be noted that the phase transition in most cases occurs at density $\rho_0 \sim 5\rho_0$, where the EOS of SQM are considered to be an important factor affecting the properties of hybrid stars [21,29]. On the other hand, the stiffened EOS can increase the baryon density of the hadron-quark phase transition, which leads to the gradual weakening of the role of quark matter for hybrid stars.

Compared with the hadronic matter (HM), SQM is known to exhibit markedly different properties. For example, SQM at very high densities ($\rho_B \geq 40\rho_0$) is approximately scale invariant or conformal, whereas in HM the degree of freedom is smaller and the scale invariance is also violated by the breaking of chiral symmetry. These qualitative differences between HM and SQM can be reflected in the different physical quantities. The sound velocity c_s, which can be calculated from $c_s^2 = \partial P/\partial\varepsilon$, takes the constant $c_s^2 = 1/3$ in the exactly conformal matter corresponding to SQM at high densities. However, c_s^2 in HM varies considerably: below saturation density, most hadronic models, such as chiral effective field theory, indicate $c_s^2 \ll 1/3$, while at higher densities the maximum of c_s^2 is predicted to be greater than 0.5 [72,73]. Another physical quantity is the polytropic index $\gamma = d(\ln P)/d(\ln\varepsilon)$, which is considered to be a good approximate criterion for the evidence of SQM in neutron stars. The polytropic index has the value $\gamma = 1$ in conformal matter, while the hadronic models generically predict $\gamma \approx 2.5$ around the saturation density [74].

In Fig. 3(a), we show the squared speed of sound c_s^2 as a function of the baryon density for hybrid star matter with the hadron-quark phase transition by varying the coupling constants g from the quasiparticle model. With the increase of g in the hadron-quark mixed phase, the curve increases rapidly and reaches a larger peak. Meanwhile, we can see that c_s^2 in the quark phase is insensitive to g, and slowly approaches the value $c_s^2 = 1/3$ of conformal matter in the high density. It should be noted that a step change of the sound velocity occurs in the hadron-quark phase transition. The speed of sound suddenly decreases at the onset of the

phase transition where the quarks appear and thus soften the EOS as a result of more degrees of freedom, and it is restored with the decrease of nucleon and lepton degrees of freedom in the high density quark phase. Further, the step change of the sound velocity in hadron-quark phase transition is relevant to the frequency of the main peak of the postmerger gravitational wave (GW) spectrum (f_2), which is expected to be confirmed by future kilohertz GW observations with third-generation GW detectors [7]. In Fig. 3(b), we show the relation between the polytropic index γ and the squared speed of sound c_s^2 in hybrid star matter. It can be seen that at saturation density c_s^2 and γ are respectively 0.08 and 2.55 from the ImMDI model with a fixed parameter set, $x = -0.3$, $y = 32$ MeV, and $z = 0$, which are consistent with those in most hadronic models. Both c_s^2 and γ in the high density quark phase approach the conformal matter limit. Our results also agree with the approximate rule following Ref. [4] that the polytropic index $\gamma \leq 1.75$ can be used as a criterion for separating hadronic from quark matter.

The mass-radius relation of hybrid stars is shown in Fig. 4, based on the quasiparticle model for SQM with the different coupling constants g. The constraints from the Bayesian analyses of the observational data from the pulsars PSR J0030 + 0451 [12,13] and PSR J0740 + 6620 [15,16], and from the analyses of the gravitational-wave signal from the neutron star merger GW170817 [17] are shown for comparison. The results shown in Fig. 4 indicate that both the observed maximum mass and corresponding radius of hybrid stars increase considerably with the coupling constant g, which is due to the maximum mass of hybrid stars constraining mostly the EOS of hybrid star matter at densities $2\rho_0 \sim 5\rho_0$ [29]. As shown in Fig. 3, the hadron-quark mixed phase in most cases occurs at this density region, and thus the properties of SQM affect the maximum mass. As a result, the maximum mass of hybrid stars increases from 1.51 to

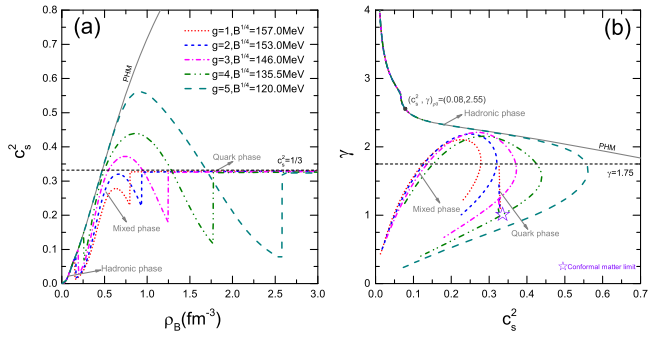

FIG. 3. The squared speed of sound c_s^2 as a function of the baryon density (a), and the relation between the polytropic index γ and the squared speed of sound c_s^2 (b) for hybrid star matter by varying the coupling constants g from the quasiparticle model. The dashed lines $c_s^2 = 1/3$ and $\gamma = 1.75$, as well as the violet star indicating the high-density conformal matter limit are also shown for comparison.

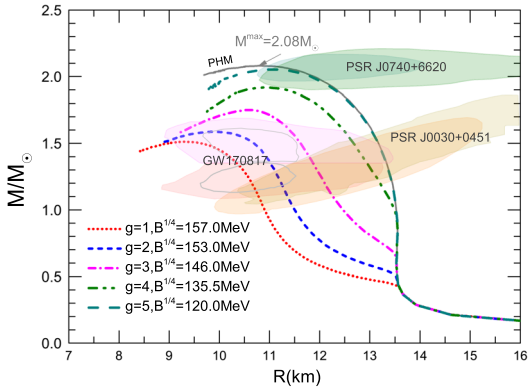

FIG. 4. Mass-radius relation of hybrid stars based on the quasiparticle model for SQM with the different coupling constants g. Constraints from multimessenger astronomy observations [12,13,15–17] are shown by shaded regions; see text for details.

$2.06M_\odot$ with the increasing g. Additionally, we also note that the maximum mass of hybrid stars with parameter sets, $g = 5$, $B^{1/4} = 120.0$ MeV and $g = 4$, $B^{1/4} = 135.5$ MeV, are very close to the detection result of PSR J0740 + 6620, and the results of hybrid stars in all parameter sets are mostly consistent with the constraints from the pulsars PSR J0030 + 0451 and the neutron star merger GW170817.

After the GW170817 event, much effort has been devoted to constraining the EOS by comparing various calculations with the range of tidal deformability. Reams of studies have examined the effects on the nuclear matter [75–77], and some of them have extracted constraints on the slope parameter $L(\rho_0)$, i.e., $L(\rho_0) = 57.7 \pm 19$ MeV [53]. The measurements of the tidal deformability of neutron stars constrain not only the EOS of dense nuclear matter but also the fundamental strong interactions of quark matter. Shown in Fig. 5 is the dimensionless tidal deformability as functions of mass and radius calculated using the different coupling constants from the quasiparticle model. We see that Λ decreases/increases rapidly as the mass/radius of the neutron star increases, which is due to the fact that given the smaller range of allowed radii for massive stars, the spread in the tidal deformability is also naturally much tighter. As expected, increasing g can stiffen the EOS of hybrid star matter and thus increase the value of the tidal deformability. Both the error bars at $M = 1.4M_\odot$ in the left panel and the squared regions in the right panel are derived from the constraints $\Lambda_{1.4} \leq 800$ and $10.5 \leq R_{1.4} \leq 13.3$ km based on the analyses of GW170817 [17,19] and the predictions of $292 \leq \Lambda_{1.4} \leq 680$ and $11.5 \leq R_{1.4} \leq 13.6$ km from heavy-ion collisions [78]. The constraint $70 \leq \Lambda_{1.4} \leq 580$ is derived from the improved analyses of Ref. [19] under several assumptions, in particular the same EOS for both stars, which is probably not the case if one of them is hybrid stars. Therefore, this constraint is not robust for hybrid stars. In this work, we only consider the range of

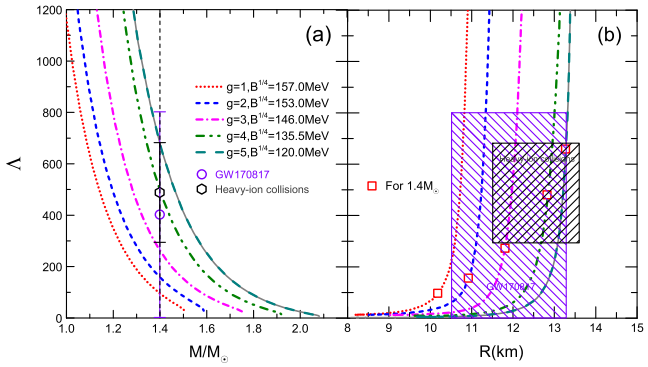

FIG. 5. Relations between the dimensionless tidal deformability and the mass as well as between the dimensionless tidal deformability and the radius in hybrid stars with the different coupling constants g for SQM. Both the error bars at $M = 1.4M_\odot$ (a) and the squared regions (b) are derived from the constraints $\Lambda < 800$ and $10.5 \leq R_{1.4} \leq 13.3$ km based on the improved analysis of GW170817 [17,19] and the predictions of $292 \leq \Lambda_{1.4} \leq 680$ and $11.5 \leq R_{1.4} \leq 13.6$ km from heavy-ion collisions [78]. The small red squares indicate the results for hybrid stars with $1.4M_\odot$.

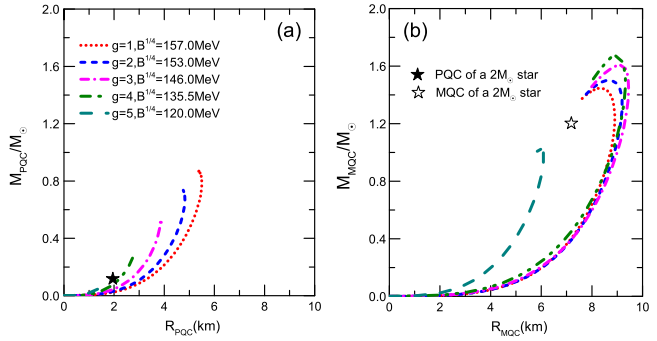

FIG. 6. Mass-radius relations the PQC and the MQC inside hybrid stars based on the quasiparticle model for SQM with different coupling constants g. The solid and void stars represent PQC and MQC of a $2M_\odot$ hybrid star, respectively.

tidal deformabilities $\Lambda < 800$ as a comparison for hybrid stars. Except for the case $g = 1$, $B^{1/4} = 157.0$ MeV, it can be seen that for the canonical mass $\Lambda_{1.4}$ and $R_{1.4}$ with various parameters meet the constraints listed above. In particular, the results of the case, $g = 4$, $B^{1/4} = 135.5$ MeV, are approaching the overlapping part of the two constraints.

The hybrid star matter EOS consists of charge-neutral matter in β-equilibrium that has a hadron-quark phase transition from hadronic to quark matter. To better understand the effects of SQM on the hybrid stars, the relation between the quark-matter core mass M_{QC} and radius R_{QC} is shown in Fig. 6. Owing to the existence of quark matter in the hadron-quark mixed phase, the discussion of the quark-matter core can be divided into two scenarios: the pure quark core (PQC) and the mixed quark core (MQC), where MQC includes the quark phase and mixed phase. The quark matter cores can be determined using the TOV equations by integrating them from the central baryon density to three distinct points: (1) the pressure of onset of pure quark phase where $r = R_{\rm PQC}$ and $M(r) = M_{\rm PQC}$, (2) the pressure of onset of mixed phase where $r = R_{\rm MQC}$ and $M(r) = M_{\rm MQC}$, and (3) zero pressure where $r = R$ and $M(r) = M$. It is clearly seen in Fig. 6(a) that the coupling constant g has a competitive effect: while the constant g increases the hybrid star mass up to $2M_\odot$, it also decreases the PQC mass $M_{\rm PQC}$ and radius $R_{\rm PQC}$. This can be understandable since the onset of the phase transition and the pure quark phase appear at higher densities with increasing g under the Gibbs construction. Particularly, if g is large enough, the onset density of quark matter will be larger than the central density of the massive stars, and thus no PQC can appear in the hybrid stars. With different coupling constants, the maximum mass and radius of PQCs, in current work, are about $0.88M_\odot$ and 5.5 km, respectively. However, the mass-radius relation of MQCs in Fig. 6(b) shows a more complex dependence: the maximum mass and radius of MQCs begin to increase gradually and decrease rapidly after reaching the maximum values with the increase of the constants g. The reason for the special dependency is that the mass and radius of MQC with small value g are in close proximity to those of the whole star, which limits the increase of the mass and radius of MQC. For the above $2M_\odot$ hybrid stars, the maximum radius of PQCs may only be about $R_{\rm PQC} \approx 2.0$ km, while the maximum radius of MQCs (the core where quark matter may appear) can be up to 7.2 km, which is over the quark core radius $R_{QC} = 6.5$ km observed in Ref. [4].

The discussion above has established that changes in B and g can significantly impact the properties of SQM and hybrid stars. Figure 7(a) displays the energy per nucleon (E/A) of SQM and udQM on the $g - B^{1/4}$ plane. The red dash-dotted line represents an E/A of 930 MeV for SQM, while the black dashed line corresponds to an E/A of 930 MeV for udQM. The slash shaded area between the two $E/A = 930$ MeV lines represents the region where absolutely stable SQM exists, which decreases as g increases and eventually narrows down to a "point" with $g = 5.62$. Hybrid stars containing SQM should break the absolutely stable condition, and the E/A of both udQM and SQM must exceed the lowest E/A value of 930 MeV. As a result, the slash and grid shaded regions represent areas excluded for hybrid stars. Consequently, the color-marked points on the red dash-dotted line with $g < 5.62$, and those on the black dashed line with $g > 5.62$ signify the minimum values of the bag constants B with different g. Our calculations also reveal that the maximum mass of hybrid stars decreases with increasing B by fixing the constant g since the bag constant B can soften the EOS of SQM through the pressure expression in Eq. (5), while the results of the radius $R_{1.4}$ and tidal deformability $\Lambda_{1.4}$ demonstrate oppositely. Therefore, we can provide the maximum mass,

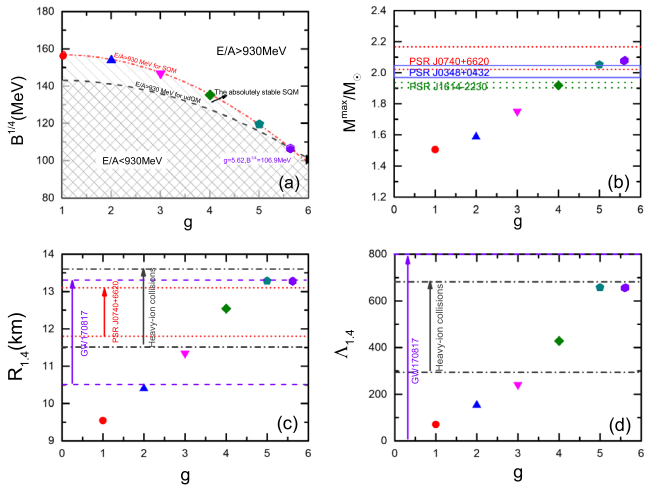

FIG. 7. Bag constant B (a), maximum mass of hybrid stars (b), as well as radius $R_{1.4}$ (c) and tidal deformability $\Lambda_{1.4}$ (d) for $1.4M_\odot$ hybrid stars as functions of the coupling constant g in the quasiparticle model. The horizontal bars in (b) indicate the observational constraints of PSR J1614-2230 [8,10], PSR J0348 + 0432 [11], and PSR J0740 + 6620 [14,16], and the horizontal bars in (c) and (d) are derived from the improved analyses of GW170817 [19] and the predictions from heavy-ion collisions [78].

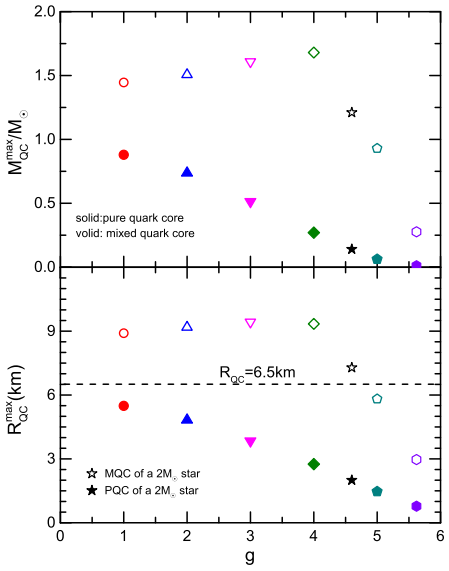

FIG. 8. Maximum mass and radius of quark-matter cores inside hybrid stars as functions of the coupling constant g in the quasiparticle model. The solid and void geometries represent the pure quark cores and mixed quark cores of the hybrid stars respectively, and the dashed line represents a 6.5 km quark core observed in Ref. [4].

minimum radius $R_{1.4}$ and minimum tidal deformation $\Lambda_{1.4}$ of the hybrid stars with different g, as shown in Figs. 7(b)–7(d). We can also see from the figures that the maximum mass, radius ($R_{1.4}$), and tidal deformability ($\Lambda_{1.4}$) increase with an increase in g. However, it should be noted that different bag constants B when $g > 5$ had no impact on the radii and tidal deformabilities of $1.4M_\odot$ hybrid stars since there is no quark matter present inside the stars. For comparison, we depict some constraints in panel (b) from the mass measurements of PSR J1614-2230 ($1.908 \pm 0.016M_\odot$) [8,10], PSR J0348 + 0432 ($2.01 \pm 0.04M_\odot$) [11], and PSR J0740+6620 ($2.08 \pm 0.07M_\odot$) [14,16], and the horizontal bars in panels (c) and (d) derived from the improved analyses of GW170817 [19] and the predictions from heavy-ion collisions [78]. It is clearly seen that the cases of $g = 4$ with various B largely satisfy all the constraints listed.

Finally, we show in Fig. 8 the maximum mass and radius of quark-matter cores inside hybrid stars as functions of the coupling constant g with the minimum B in the quasiparticle model. We can see in the figures that the maximum mass and radius of PQCs decreases with the increment of g, whereas those of MQCs begin to increase gradually and decrease rapidly after reaching the maximum values with the increase of the constants g. Different from the complete stars, both the maximum mass and radius of PQCs and MQCs have a negative dependence on the bag constant B by fixing the constant g, and thus the mass and radius of PQCs and MQCs in Fig. 8 correspond to the maximum values with different g. For the $2M_\odot$ stars with the hadron-quark phase transition, the radii of quark-matter cores observed in Ref. [4] can reach about 6.5 km as shown by the dashed line in Fig. 8. It is clearly seen in Fig. 8 that the PQCs of the massive stars gradually scale down or even nearly disappear. Especially for the extreme value $g = 5.62$, the star mass can be up to $2.08M_\odot$, whereas the PQC mass almost approaches zero, and its radius is also less than 1 km. By contrast, considering the mixed phase, the sizable quark-matter cores ($R_{\mathrm{MQC}} > 6.5$ km) can appear in $2M_\odot$ massive stars.

IV. SUMMARY AND OUTLOOK

In this work, we have investigated the global properties of hybrid stars with the hadron-quark phase transition based on the quasiparticle model. In conclusion, we find that the hybrid star matter EOS is sensitive to the strength of the constants g. With increasing the coupling constant g the EOS of hybrid star matter becomes stiffer. Meanwhile, we also note that a step change of the sound velocity occurs in the hadron-quark phase transition. The speed of sound suddenly decreases at the onset of the phase transition, and it is restored with the decrease of nucleon and lepton degrees of freedom in the high density quark phase. Our results agree with the approximate rule following Ref. [4] that the polytropic index $\gamma \leq 1.75$ can be used as a criterion for separating hadronic from quark matter. Using the hybrid star matter EOS, we predict the mass-radius relation and tidal deformabilities of hybrid stars as well as the radius and mass information

of quark-matter cores. Although the constant g increases the hybrid star maximum mass up to $2.08M_\odot$, it also decreases the mass and radii of quark-matter cores. However, considering the quark matter in the mixed phase, we confirm that the sizable quark-matter core $R_{QC} = 7.2$ km can appear in $2M_\odot$ massive stars.

The hypothesis of absolutely stable SQM suggests that the SQM in hybrid stars should break the absolutely stable condition, and the energy per nucleon (E/A) of both udQM and SQM must exceed the lowest energy per nucleon 930 MeV. In the work, we present the energy per nucleon (E/A) of SQM and udQM and regions excluded for hybrid stars on the $g - B^{1/4}$ plane. We find that the maximum mass of hybrid stars decreases with increasing B since the bag constant B can soften the EOS of SQM, while the results of the radius $R_{1.4}$ and tidal deformability $\Lambda_{1.4}$ for a $1.4M_\odot$ star demonstrate oppositely. Different from the complete stars, both maximum mass and radius of quark-matter cores have a negative dependence on the bag constant B. As a result, we provide the maximum mass, minimum radius $R_{1.4}$, and tidal deformation $\Lambda_{1.4}$ of the hybrid stars as well as the maximum mass and radius of the quark matter core with different g values within the allowable regions ($E/A > 930$ MeV) on the $g - B^{1/4}$ plane. For comparison, we also display some constraints from astrophysical observations and heavy-ion experiments, which comprise the multimessenger data set for our analyses on the properties of hybrid star matter. In addition, some of the new discoveries and observations provide more rigorous constraints on SQM, or may also contain some new physics, for example, the newly discovered compact binary merger GW190814 with a secondary component of mass $2.50 \sim 2.67M_\odot$, which can be reproduced by a superfast pulsar [79] or quark star [44,45]. Those observations of massive stars can also be used to understand the properties of the QCD phase transition. To further explore the QCD phase structure and search for the signal of the QCD critical point, experimental programs such as the beam-energy scan at RHIC were proposed. The promising results are available to provide more constraints on the EOSs of SQM, and are helpful in the understanding of the QCD phase structure.

ACKNOWLEDGMENTS

This work is supported by the National Natural Science Foundation of China under Grants No. 12205158 and No. 11975132, and the Shandong Provincial Natural Science Foundation, China Grants No. ZR2021QA037, No. ZR2022JQ04, No. ZR2019YQ01, and No. ZR2021MA037.

[1] N. K. Glendenning, Phys. Rep. **342**, 393 (2001).
[2] F. Weber, Prog. Part. Nucl. Phys. **54**, 193 (2005).
[3] Y. Aoki, G. Endrődi, Z. Fodor, S. D. Katz, and K. K. Szabó, Nature (London) **443**, 675 (2006).
[4] E. Annala, T. Gorda, A. Kurkela, J. Nättilä, and A. Vuorinen, Nat. Phys. **16**, 907 (2020).
[5] M. G. Alford, S. Han, and K. Schwenzer, J. Phys. G **46**, 114001 (2019).
[6] A. Bauswein, N. F. Bastian, D. B. Blaschke, K. Chatziioannou, J. A. Clark, T. Fischer, and M. Oertel, Phys. Rev. Lett. **122**, 061102 (2019).
[7] Y. J. Huang, L. Baiotti, T. Kojo, K. Takami, H. Sotani, H. Togashi, T. Hatsuda, S. Nagataki, and Y. Z. Fan, Phys. Rev. Lett. **129**, 181101 (2022).
[8] P. B. Demorest, T. Pennucci, S. M. Ransom, M. S. E. Roberts, and J. W. T. Hessels, Nature (London) **467**, 1081 (2010).
[9] E. Fonseca, T. T. Pennucci, J. A. Ellis *et al.*, Astrophys. J. **832**, 167 (2016).
[10] Z. Arzoumanian, P. T. Baker, A. Brazier *et al.*, Astrophys. J. **859**, 47 (2018).
[11] J. Antoniadis, P. C. C. Freire, N. Wex *et al.*, Science **340**, 448 (2013).
[12] T. E. Riley, A. L. Watts, S. Bogdanov *et al.*, Astrophys. J. Lett. **887**, L21 (2019).
[13] M. C. Miller, F. K. Lamb, A. J. Dittmann *et al.*, Astrophys. J. Lett. **887**, L24 (2019).
[14] H. T. Cromartie, E. Fonseca, and S. M. Ransom *et al.*, Nat. Astron. **4**, 72 (2020).
[15] T. E. Riley, A. L. Watts, and, P. S. Ray *et al.*, Astrophys. J. Lett. **918**, L27 (2021).
[16] M. C. Miller, F. K. Lamb, A. J. Dittmann *et al.*, Astrophys. J. Lett. **918**, L28 (2021).
[17] B. P. Abbott *et al.* (LIGO Scientific and Virgo Collaborations), Phys. Rev. Lett. **119**, 161101 (2017).
[18] B. P. Abbott *et al.* (LIGO Scientific and Virgo Collaborations), Astrophys. J. Lett. **896**, L44 (2020).
[19] B. P. Abbott *et al.* (LIGO Scientific and Virgo Collaborations), Phys. Rev. Lett. **121**, 161101 (2018).
[20] J. Lattimer and M. Prakash, Phys. Rep. **333**, 121 (2000).
[21] W. J. Xie and B. A. Li, Astrophys. J. **899**, 4 (2020).
[22] P. Danielewicz, R. Lacey, and W. G. Lynch, Science **298**, 1592 (2002).
[23] C. Fuchs, Prog. Part. Nucl. Phys. **56**, 1 (2006).
[24] M. G. Alford, S. Han, and M. Prakash, Phys. Rev. D **88**, 083013 (2013).
[25] G. Montana, L. Tolos, M. Hanauske, and L. Rezzolla, Phys. Rev. D **99**, 103009 (2019).
[26] J. J. Li, A. Sedrakian, and M. Alford, Phys. Rev. D **101**, 063022 (2020).

[27] N. B. Zhang and B. A. Li, Astrophys. J. **921**, 111 (2021).
[28] O. Ivanytskyi and D. Blaschke, Phys. Rev. D **105**, 114042 (2022).
[29] H. Liu, J. Xu, and P. C. Chu, Phys. Rev. D **105**, 043015 (2022).
[30] J. Xu, L. W. Chen, and B. A. Li, Phys. Rev. C **91**, 014611 (2015).
[31] J. Xu, A. Carbone, Z. Zhang, and C. M. Ko, Phys. Rev. C **100**, 024618 (2019).
[32] N. K. Glendenning, Phys. Rev. D **46**, 1274 (1992).
[33] E. Witten, Phys. Rev. D **30**, 272 (1984).
[34] G. Baym, E. W. Kolb, L. McLerran, T. P. Walker, and R. L. Jaffe, Phys. Lett. **160B**, 181 (1985).
[35] A. V. Olinto, Phys. Lett. B **192**, 71 (1987).
[36] T. Fischer, I. Sagert, G. Pagliara, M. Hempel, J. Schaffner-Bielich, T. Rauscher *et al.*, Astrophys. J. Suppl. Ser. **194**, 39 (2010).
[37] J. Xu, L. W. Chen, C. M. Ko, and B. A. Li, Phys. Rev. C **81**, 055803 (2010).
[38] S. Weissenborn, I. Sagert, G. Pagliara, M. Hempel, and J. Schaffner-Bielich, Astrophys. J. Lett. **740**, L14 (2011).
[39] E. Hiyama, K. Sasaki, T. Miyamoto, T. Doi, T. Hatsuda, Y. Yamamoto, and Th. A. Rijken, Phys. Rev. Lett. **124**, 092501 (2020).
[40] L. Contessi, N. Barnea, and A. Gal, Phys. Rev. Lett. **121**, 102502 (2018).
[41] C. Manuel, Phys. Rev. D **53**, 5866 (1996).
[42] K. Schertler, C. Greiner, and M. H. Thoma, Nucl. Phys. **A616**, 659 (1997).
[43] X. J. Wen, Z. Q. Feng, N. Li, and G. X. Peng, J. Phys. G **36**, 025011 (2009).
[44] P. C. Chu, Y. Y. Jiang, H. Liu, Z. Zhang, X. M. Zhang, and X. H. Li, Eur. Phys. J. C **81**, 569 (2021).
[45] Z. Zhang, P. C. Chu, X. H. Li, H. Liu, and X. M. Zhang, Phys. Rev. D **103**, 103021 (2021).
[46] M. A. van Eijck, C. R. Stephens, and C. G. van Weert, Mod. Phys. Lett. A **8**, 309 (1994).
[47] M. I. Gorenstein and S. N. Yang, Phys. Rev. D **52**, 5206 (1995).
[48] B. K. Patra and C. P. Singh, Phys. Rev. D **54**, 3551 (1996).
[49] A. Carbone, A. Rios, and A. Polls, Phys. Rev. C **90**, 054322 (2014).
[50] A. Carbone, A. Polls, and A. Rios, Phys. Rev. C **98**, 025804 (2018).
[51] C. Wellenhofer, J. W. Holt, and N. Kaiser, Phys. Rev. C **92**, 015801 (2015).
[52] C. Wellenhofer, J. W. Holt, and N. Kaiser, Phys. Rev. C **93**, 055802 (2016).
[53] B. A. Li, B. J. Cai, W. J. Xie, and N. B. Zhang, Universe **7**, 182 (2021).
[54] J. Estee *et al.* (SpRIT Collaboration). Phys. Rev. Lett. **126**, 162701 (2021).
[55] D. Adhikari *et al.* (PREX Collaboration), Phys. Rev. Lett. **126**, 172502 (2021).
[56] B. T. Reed, F. J. Fattoyev, C. J. Horowitz, and J. Piekarewicz, Phys. Rev. Lett. **126**, 172503 (2021).
[57] M. B. Tsang, J. R. Stone, F. Camera, P. Danielewicz, S. Gandolfi, K. Hebeler *et al.*, Phys. Rev. C **86**, 015803 (2012).
[58] J. M. Lattimer and Y. Lim, Astrophys. J. **771**, 51 (2013).
[59] T. Maruyama, S. Chiba, H.-J. Schulze, and T. Tatsumi, Phys. Rev. D **76**, 123015 (2007).
[60] X. Na, R. Xu, F. Weber, and R. Negreiros, Phys. Rev. D **86**, 123016 (2012).
[61] X. H. Wu and H. Shen, Phys. Rev. C **99**, 065802 (2019).
[62] G. Lugones and A. G. Grunfeld, Phys. Rev. D **104**, L101301 (2021).
[63] M. Ju, X. H. Wu, F. Ji, J.-N. Hu, and H. Shen, Phys. Rev. C **103**, 025809 (2021).
[64] J. Xu, L. W. Chen, B. A. Li, and H. R. Ma, Phys. Rev. C **79**, 035802 (2009).
[65] J. Xu, L. W. Chen, B. A. Li, and H. R. Ma, Astrophys. J. **697**, 1549 (2009).
[66] J. Carriere, C. J. Horowitz, and J. Piekarewicz, Astrophys. J. **593**, 463 (2003).
[67] G. Baym, C. Pethick, and P. Sutherland, Astrophys. J. **170**, 299 (1971).
[68] T. Hinderer, Astrophys. J. **677**, 1216 (2008); **697**, 964(E) (2009).
[69] J. S. Read, C. Markakis, M. Shibata, K. B. O. Uryu, J. D. E. Creighton, and J. L. Friedman, Phys. Rev. D **79**, 124033 (2009).
[70] S. Postnikov, M. Prakash, and J. M. Lattimer, Phys. Rev. D **82**, 024016 (2010).
[71] E. Farhi and R. L. Jaffe, Phys. Rev. D **30**, 2379 (1984).
[72] S. Gandolfi, A. Yu. Illarionov, K. E. Schmidt, F. Pederiva, and S. Fantoni, Phys. Rev. C **79**, 054005 (2009).
[73] I. Tews, T. Krüger, K. Hebeler, and A. Schwenk, Phys. Rev. Lett. **110**, 032504 (2013).
[74] A. Kurkela, P. Romatschke, and A. Vuorinen, Phys. Rev. D **81**, 105021 (2010).
[75] P. G. Krastev and B. A. Li, J. Phys. G **46**, 074001 (2019).
[76] Z. Carson, A. W. Steiner, and K. Yagi, Phys. Rev. D **99**, 043010 (2019).
[77] N. B. Zhang and B. A. Li, Eur. Phys. J. A **55**, 39 (2019).
[78] B. A. Li and A. W. Steiner, Phys. Lett. B **642**, 436 (2006).
[79] N. B. Zhang and B. A. Li, Astrophys. J. **902**, 38 (2020).